Published in final edited form as:
J Bone Miner Res. 2012 December ; 27(12): 2573–2581. doi:10.1002/jbmr.1709.

Deuterium nuclear magnetic resonance unambiguously quantifies pore and collagen-bound water in cortical bone

Henry H. Ong, Ph.D., **Alexander C. Wright, Ph.D.**, and **Felix W. Wehrli, Ph.D.**
Laboratory for Structural NMR Imaging, Department of Radiology, University of Pennsylvania School of Medicine, Philadelphia, PA

Abstract

Bone water (BW) plays a pivotal role in nutrient transport and conferring bone with its viscoelastic mechanical properties. BW is partitioned between the pore spaces of the Haversian and lacuno-canalicular system, and water predominantly bound to the matrix proteins (essentially collagen). The general model of BW is that the former predominantly experiences fast isotropic molecular reorientation, whereas water in the bone matrix undergoes slower anisotropic rotational diffusion. Here, we provide direct evidence for the correctness of this model and show that unambiguous quantification *in situ* of these two functionally and dynamically different BW fractions is possible.

The approach chosen relies on nuclear magnetic resonance (NMR) of deuterium (^{2}H) that unambiguously separates and quantifies the two fractions on the basis of their distinguishing microdynamic properties. Twenty-four specimens of the human tibial cortex from six donors (3 male, 3 female, ages 27-83 years) were cored and ^{2}H spectra recorded at 62 MHz (9.4 Tesla) on a Bruker Instruments DMX 400 spectrometer after exchange of native BW with ^2H_2O. Spectra consisted of a doublet signal resulting from quadrupole interaction of water bound to collagen. Doublet splittings were found to depend on the orientation of the osteonal axis with respect to the magnetic field direction (8.2 and 4.3 kHz for parallel and perpendicular orientation, respectively). In contrast, the isotropically reorienting pore-resident water yielded a single resonance line superimposed on the doublet. Nulling of the singlet resonance allowed separation of the two fractions. The results indicate that in human cortical bone 60-80% of detectable BW is collagen-bound. Porosity determined as the difference between total BW and collagen bound water fraction was found to strongly parallel μCT based measurements ($R^2 = 0.91$). Our method provides means for direct validation of emerging relaxation-based measurements of cortical bone porosity by proton MRI.

Keywords

cortical bone; bone water; porosity; deuterium NMR; MRI

Introduction

Bone is a living, composite material consisting of a mineral phase of nonstoichiometric calcium apatite and an organic phase composed predominantly of type-I collagen (1). Cortical or compact bone, comprising 80% of the skeleton's mass, has a characteristic pore

Correspondence and **Request for Reprints**: Felix W. Wehrli, University of Pennsylvania Medical Center, 1 Founders, MRI Education Center, 3400 Spruce Street, Philadelphia, PA 19104, Tel: 215-662-7951, Fax: 215-662-7263, wehrli@mail.med.upenn.edu.

Disclosure
All authors state that they have no conflicts of interest.

structure consisting of channels (Haversian and Volkmann's canals) housing the blood supply and accounting for over 90% of the total pore volume (2). Smaller pores comprising osteocyte-containing lacunae and canaliculi, which allow for communication between lacunae and vascular channels, make up the balance of the pore space. Next to the organic matrix and mineral phase, water occupies the largest fraction in compact bone, accounting for 10-20% of its wet weight (3). Bone water (BW) functions include nutrient transport (4), conferring to bone its viscoelastic properties (5), and regulating bone formation through mechanosensory pathways (6). It is therefore understandable that the nature and function of BW has been studied extensively (3,7-12).

Knowledge of BW is of substantial interest as it can provide insight into mechanical properties of bone. BW can be found in the pore space within bone (i.e. 'pore BW') and in the bone matrix, where it is associated with the mineral (13-15) and organic phases (16-19). Pore BW is of particular importance as it can provide a surrogate marker for porosity, which cannot directly be measured because most pore sizes are below the resolution limit of *in vivo* imaging devices. Porosity is of clinical relevance as it is an important predictor of cortical bone's mechanical competence and thus fracture susceptibility (20).

Magnetic resonance imaging (MRI) is uniquely capable of directly detecting and quantifying BW *in vivo* and assessing its spatial distribution in the skeleton (21-24). As the MR signal of BW is very short-lived with relaxation rates, $T^*_2 < 1$ ms, a phenomenon accounted to restricted mobility and spatial variations in magnetic susceptibility, conventional MRI is unable to detect BW. During recent years MRI methods have emerged that allow spatial encoding to start tens of microseconds or less after radio-frequency (RF) excitation. Key among these are ultra-short echo-time (UTE) (25), zero echo-time (26-27), and sweep imaging with Fourier transform (28). One difficulty with these methods is that the proton signal in bone can arise from several different populations of protons (i.e. collagen, lipids, pore BW etc.), each with its own relaxation characteristics. Depending on the specific acquisition method, different proton populations may be detected.

It has recently been reported that the proton MR signal of pore BW is confounded by BW in the bone matrix (29). Since the very small fraction of mineral-associated BW relaxes too fast to be detected with MRI (14), the large majority of matrix-associated BW is bound to the organic phase (i.e. 'collagen-bound BW'). Bulk BW concentration (BWC, essentially the sum of the concentrations of pore and collagen-bound BW), has been shown to be an inadequate predictor of the bone's mechanical parameters (30). This may be explained by pore BW fraction being inversely related to collagen BW fraction, i.e. pore volume increases as bone matrix volume decreases, which clearly complicates interpretation of bulk BWC measurements.

In order to understand the biophysical and biomechanical significance of bulk BWC, separation of collagen-bound and pore BW signals is required. Such a separation would also be the first step toward true bone porosity measurement with MRI. Various approaches have recently been proposed for such a separation via UTE-MRI (31-33). These approaches are based on the expected difference in relaxation properties between collagen-bound and pore BW. In the former, BW forms hydrogen bonds with collagen and experiences slow anisotropic motion (34) leading to enhanced transverse relaxation ($1/T_2$, $1/T^*_2$) (29) (i.e. 'bound water'). Pore BW can be thought of as bulk water that experiences isotropic reorientation leading to longer T_2 and T^*_2 (i.e. 'free water'). Note that given the low concentration of lipids in cortical bone (29) and the short T^*_2 of collagen protons (35), lipids and collagen are not usually detected with UTE-MRI.

The underlying assumption in this relaxation model, which has not been empirically validated, is that pore BW is predominantly free while water in the bone matrix is predominantly bound. It is conceivable that pore BW could have some bound components in the form of intracellular water in osteocytes associated with macro-molecules. Likewise, the bone matrix could contain free water in micro-pores, i.e. spaces between collagen fibers, much like in hydrated tendon (36), or between the organic and mineral phases (37).

NMR relaxometry, as described below, has been used to support the above relaxation model. As there is no physical boundary between collagen-bound and pore BW, a fundamental assumption underlying NMR relaxometry is that the exchange between the two BW populations is slow on the NMR timescale, in which case the free induction decay (FID) can be regarded as a weighted sum of exponentials differing in decay time-constants (T^*_2). Similarly, the echo envelope from a Carr-Purcell-Meiboom-Gill (CPMG) experiment (38) can be thought of as a weighted sum of echo amplitudes, each pertaining to a particular T_2. Applying a Laplace inversion to the measured overall FID or echo decay will then produce a T^*_2 or T_2 spectrum, respectively.

At the relatively low magnetic field of 0.6T the T^*_2 spectrum from human femoral cortical bone revealed three peaks at around 0.01, 0.3 and 3 ms, which were attributed to protons from collagen, collagen-bound BW, and BW in pore spaces (39-40). Interestingly, there have been conflicting reports as to whether this observation holds at higher magnetic field (29,31,33), which emphasizes the need for unambiguous quantification of collagen-bound and pore BW. T_2 spectra acquired at various field strengths (0.05-4.7 T) suggest $T_2 > 1$ ms to arise predominantly from BW in the pore spaces (29,41-42). The authors in (29) postulated T_2 on the order of 400 μs to result from both collagen-bound and pore BW.

The inherent difficulty in these BW assignments is that they are inferential in nature in that there is no direct evidence for a given T^*_2 or T_2 component to correspond with collagen-bound or pore BW. Assignments are based on *a priori* assumptions on the expected relaxation characteristics as described above. Furthermore, a fundamental challenge in NMR relaxometry is that the Laplace inversion is an ill-conditioned transformation (43-44). Consequently, noise can lead to widely varying results, and, most importantly, there are no *unique* T^*_2 and T_2 spectra for a given FID or CPMG echo decay envelope. The inversion process must be carefully done in order to ensure robustness in the results.

In this work, we conceived an NMR method to unambiguously distinguish and quantify bound and free water in bone by exploiting differences in spectral, as opposed to relaxometric, behavior between isotropic and anisotropic molecular motion. We validated the method through comparisons to micro-computed tomography (μCT) measurements of cortical bone porosity.

Methods and Materials

Bone Specimens

Lamb cortical bone specimens were harvested from shanks purchased from a local grocer (6-8 month old lamb). Twenty-four human cortical bone specimens were harvested from the tibiae of three male and three female donors of various ages (27–83 years old; Musculoskeletal Transplant Foundation (www.mtf.org) and National Disease Research Interchange (www.nrdriresource.org)). The human tibia specimens were unfixed and frozen within 24 hours post-mortem. All donors were healthy and did not have any known bone-related diseases.

Using a Dremel rotary tool with a cut-off wheel attachment (www.dremel.com), bone specimens were cut and ground into approximately cylindrical samples to fit into a 5mm NMR tube. Human bone samples were cut from the posterior, medial, lateral, and anterior sides at 38% of the tibial length from the distal end.

All bone specimens were stored in a refrigerator in 8.5% saline. For deuterium exchange, bone specimens were immersed in 8.5% deuterium oxide (^2H_2O) saline for 48-72 hrs prior to the ^2H NMR experiments.

NMR Experiments

As observed in tendon and cartilage, which have highly aligned collagen fibers, bound water exhibits slow anisotropic motion resulting in residual dipolar (for ^1H) or quadrupolar (for ^2H) splittings ($\Delta\nu$in Hz) in NMR spectra (36,45-46). It is reasonable to expect that bound water in bone will also exhibit these interactions and therefore display splittings whereas free water will not due to faster isotropic rotational diffusion. Here, we hypothesize that bound water is predominantly collagen-bound and free water is predominantly pore-resident.

To obtain ^2H NMR spectra, bone specimens were immersed in excess ^2H_2O, ensuing in replacement of all labile protons by deuterons (essentially native collagen-associated and pore BW). After ^2H_2O immersion, total BW content can be quantified as exchanged H_2O in the ^2H_2O immersion fluid. It has previously been shown that BW content obtained in this manner is not significantly different from conventional gravimetric methods after drying at 100°C (10).

The dipolar and quadrupolar splittings in cortical bone were first investigated using an in-phase double-quantum-filter (IP-DQF) pulse sequence (34). By varying a timing parameter (creation time, τ), this sequence can filter out the overlapping central peak from the pore BW. Splittings from lamb and human mid-tibia bone specimens were characterized with ^1H and ^2H IP-DQF NMR before and after ^2H_2O immersion.

As will be shown, residual dipolar splittings from collagen-bound BW were not observed in the proton spectra. However, due to the stronger quadrupolar interaction and temperature invariance (34), quadrupolar splitting from collagen-bound BW were readily observed. Collagen-bound and pore BW fractions in human mid-tibia bone specimens were quantified by ^2H inversion-recovery (IR) NMR after ^2H_2O immersion. It was empirically found that residual quadrupolar interactions of collagen-bound BW resulted in longitudinal relaxation considerably faster than that in pore BW, which allows for inversion nulling of the collagen-bound quadrupolar splitting signal from the central peak arising from pore BW.

After quantification, bone porosity was calculated as pore volume divided by total volume of the bone specimen. Pore volume was estimated from the total BW content measured with ^2H_2O immersion and the known density of water, whereas total bone specimen volume was measured from μCT images (see methods below).

All NMR experiments were performed on a 9.4T spectrometer (DMX-400, Bruker Instruments) and spectra were processed using the accompanying Xwin-NMR software. Bone specimens were removed from storage or immersion fluid and blotted dry before being placed into 5 mm NMR tubes.

^1H pulse-acquire experiments were run with the following parameters: Repetition time = 2s, τ_{90} = 3.4 μs, 16k data points, NS = 64, sweep width of 200 kHz. ^1H IP-DQF experiments

were run with the following parameters: repetition time = 2s, $\tau_{90}/\tau_{creation}/\ \tau_{DQ}/\ \tau_{ZQ}$ = 3.4/25-1000/20/20μs, 16k data points, NS = 64, sweep width of 200 kHz.

Total BW content was measured from the native bone water extruded after immersion in excess ^2H_2O and quantified by reference to calibration sample of various proton concentrations (10-11). A ^1H pulse-acquire experiment was performed on the immersion and calibration fluid with the following parameters: Repetition time = 2s, τ_{90} = 3.4 μs, 16k data points, NS = 64, sweep width of 25 kHz.

After deuterium exchange, ^2H pulse-acquire experiments were performed with the following parameters: repetition time = 1s, τ_{90} = 47 μs, 16k data points, NS = 5k, sweep width of 100 kHz. ^2H IP-DQF experiments were run with the following parameters: Repetition time = 1s, $\tau_{90}/\tau_{creation}/\ \tau_{DQ}/\ \tau_{ZQ}$ = 47/100-1000/20/20 μs, 16k data points, NS = 5k, sweep width of 100 kHz. ^2H IR experiments was performed with the following parameters: Repetition time = 1s, τ_{90}/τ_{180} = 47/94 μs, TI = 0.05 - 4000 *ms*, 16k data points, NS = 64, sweep width of 100 kHz.

μCT

The μCT images were acquired either with an eXplore Locus SP μCT system (GE Healthcare, Waukesha, WI, USA) or a SkyScan 1172 (SkyScan, Kontich, Belgium) scanner at a nominal resolution of 16 μm, using the following parameters: eXplore Locus SP: 80 kVp, 80 μA, 0.25 mm aluminum filter, 400 views, 0.5° increment, 2×2 bin mode, 1.7 s exposure, 16 averages, scan time 3 hrs 2 mins; SkyScan 1172: 80 kV, 75 μA, 0.25 mm aluminum filter, 500 views, 0.4° increment, 0.25 s exposure, 8 averages, scan time 34 mins. The SkyScan 1172 scanner was also used to acquire the 1 μm isotropic resolution images with the following parameters: 59 kV, 167 μA, 0.5 mm aluminum filter, 641 views, 0.3° increment, 1.5 s exposure, 12 averages, scan time 3 hr 16 mins.

All images were processed with ImageJ (NIH) to calculate total bone volume and porosity using simple thresholding, and to segment lacunae from vascular canals using shaped-based particle analysis. Volume-rendered images were generated with OsiriX software (www.osirix-viewer.com).

Results

Lamb bone specimens

Figure 1a shows ^1H pulse-acquire and IP-DQF (τ = 25μs) spectra of a fully hydrated lamb tibia cortical bone specimen. A dipolar splitting ($\Delta\omega$40kHz) is clearly observable in the IP-DQF spectrum. After full ^2H_2O exchange (Figure 1b), the central peak is reduced ten-fold, rendering the splitting more apparent. ^2H_2O exchange does not affect the IP-DQF spectrum and there is no orientational dependence (Figure 1c). Figure 1d shows ^1H IP-DQF spectra of the specimen oriented with its long axis perpendicular to B_0 for various creation times to probe splittings varying in magnitude.

Figures 1e-f display ^2H pulse-acquire and IP-DQF (τ = 200 μs) spectra of the same lamb bone specimen with the long axis of the specimen parallel ($\Delta\omega$ = 8kHz) and perpendicular ($\Delta\omega$ = 4.7kHz) to B_0 after having been equilibrated in ^2H_2O for 48-72 hrs. Figures 1 g-h show ^2H IP-DQF spectra at various creation times for the two specimen orientations. Note the appearance two splittings ($\Delta\omega$ = 8 and 2.2 kHz) at a creation time of 400μs in the parallel orientation.

Human Bone Specimens

Figure 2a displays ^{1}H pulse-acquire and IP-DQF (τ = 25μs) spectra of a human anterior tibia cortical bone specimen from a 37 year-old male donor after ^2H_2O immersion. A dipolar splitting ($\Delta\omega \approx$ 40kHz) is again clearly observable in the IP-DQF spectrum. Only the parallel orientation is shown as no dependence on orientation was observed as with the lamb specimens. Figure 2b shows ^{1}H IP-DQF spectra at various creation times and the principal loading axis of the specimen was parallel to B_0. Unlike the lamb specimens, there was a secondary residual peak observed in the ^{1}H IP-DQF spectra at τ = 200 μs (Fig 2c) that was dependent on temperature and was not observable after ^2H_2O immersion. No major differences in the above spectra were observed with changes in sex, age or anatomic location.

Figures 2d-e show ^{2}H pulse-acquire and IP-DQF (τ = 200μs) spectra of the same human bone specimen equilibrated in ^2H_2O with the long axis of the specimen parallel ($\Delta\omega$ = 8.2kHz) and perpendicular ($\Delta\omega$ = 4.3kHz) to B_0. Figure 2f shows ^{2}H IP-DQF spectra at various creation times with the long axis of the specimen parallel to B_0. Note again the appearance of two splittings ($\Delta\omega$ = 9.2 and 2.7 kHz) at a creation time of 400μs. No major differences in the above spectra were observed with changes in sex, age or anatomic location.

Figure 3a shows a series of IR spectra of the same human bone specimen at various inversion times (TI). The quadrupolar splitting is nulled at TI = 3 ms. Addition of the TI = 3 ms spectrum after correction for T_1 relaxation to the TI = 4 s spectrum (i.e. after full T_1 relaxation) yields the collagen-bound BW spectrum (Figure 3b). The pore BW spectrum is obtained by subtracting the fully relaxed spectrum obtained with TI = 4 s with the collagen-bound BW spectrum (Figure 3b). Fractions of collagen-bound and pore BW are computed from the integral areas in comparison to TI = 4 s.

Correlation plots of NMR bone porosity, bulk BWC (as defined by total BW content divided by total bone specimen volume), pore BW fraction, and collagen-bound BW fraction, versus μCT bone porosity are given in Figure 4 along with sample μCT images for each of the six donors. All correlations were significant ($p<0.0001$). NMR porosity shows the highest correlation (R^2 = 0.91) but bulk BWC yielded a strong correlation as well (R^2 = 0.73). Both pore and collagen-bound BW fraction are similarly correlated with μCT porosity (R^2= 0.76), albeit with opposite sign.

High-resolution μCT images

Figure 5 shows sample high-resolution (1 μm) μCT images of lamb and human cortical bone specimens. Vascular channels are smaller in diameter and greater in density in lamb than in human bone. Note that there are more transverse vascular channels in lamb bone. The lamb bone also shows greater and more spatially variable lacunar density, which may be indicative of the higher bone turnover rate in the younger lamb bone (47).

Discussion

^{1}H pulse-acquire and IP-DQF spectra

Both human and lamb bone ^{1}H pulse-acquire spectra clearly display a narrow peak superimposed on a broad, non-Lorentzian resonance. With the exception of the narrow central peak being greatly reduced after deuterium exchange, there were no observable differences between spectra before and after ^2H_2O immersion. The narrow central peak that remains after deuterium exchange could arise from non-exchangeable BW in micro-pores, i.e. an order of magnitude smaller than canaliculi, in the bone matrix (10) or from collagen

proton pairs oriented close to the magic-angle with respect to B_0 (48). As stated above, previous work showed that BW content measured by ^2H_2O immersion with an immersion time of ≥6 hrs was not significantly different from results obtained by gravimetry after drying at 100°C (10). It is thus fair to conclude that full exchange of the collagen-bound and pore BW could be expected for our only slightly larger bone specimens after D_2O immersion for 48 hours or longer.

The ^1H IP-DQF data for both species indicate that the broad peak is comprised of dipolar splittings that result from protons exhibiting slow anisotropic motion. The splitting decreases with increasing τ, which shows the presence of a range of dipolar interactions caused by variations in inter-nuclear distances and orientations of the proton-proton inter-nuclear distance vectors. The observation that the splittings persisted after ^2H_2O immersion and remained invariant over a range of temperatures (5-50°C) suggests that they arise from non-exchangeable protons, most likely from protons on the collagen backbone. The measured splitting ($\Delta\omega \approx 40$ kHz) at $\tau = 25\mu s$ is also in agreement with previous observations in tendon (46).

In lamb bone specimens, unlike in ^1H IP-DQF experiments on tendon where collagen fibers are collinear (36), no evidence of dipolar splitting from collagen-bound BW was seen. The dependence on inter-nuclear distance and orientation of neighboring protons makes dipolar splittings difficult to observe. Given the plywood-like collagen fiber organization in lamellar bone (49-50), the residual dipolar interaction may be further reduced. Nevertheless, in the human bone specimens, an additional residual peak was observed in the ^1H IP-DQF spectra at $\tau = 200\ \mu s$. The observations that the linewidth increased with lower temperature and the peak was not observable after ^2H_2O immersion suggests that this signal arises from exchangeable collagen-bound BW as lower temperatures lead to a stronger residual dipolar interaction (34).

This difference in spectral behavior for lamb and human bone could result from inter-species variation in matrix microstructure (51). Lamb bone is composed of both woven and lamellar bone while human home consists solely of lamellar bone. Therefore, the collagen fibers are more disorganized in lamb bone than in human bone. Increased organization leads to stronger residual dipolar interaction. Failure to observe dipolar splittings from bound BW in human bone shows that the residual dipolar interaction is extremely weak, likely due to the plywood-like collagen fiber organization in human bone (49-50).

^2H pulse-acquire and IP-DQF spectra

^2H NMR facilitates observation of quadrupole splitting from bound BW for several reasons. First, the quadrupolar interaction is significantly stronger (34). Second, the quadrupolar interaction does not depend on the spin state of neighboring nuclei and therefore can produce well-resolved spectra that are not temperature dependent (34). Third, after immersion in ^2H_2O, the ^2H signal can only arise from exchangeable hydrogen, which is predominantly made up of BW (11), i.e. the spectrum is free of background signal such as hydrogen from collagen.

The ^2H NMR spectra of human and lamb bone showed many similarities. The ^2H pulse-acquire spectra clearly display a narrow peak flanked by quadrupolar splittings indicating the presence of BW exhibiting isotropic and anisotropic rotational motion, respectively. The quadrupolar splitting in the ^2H IP-DQF spectra show little dependence on τ suggesting the existence of single dominant splitting, which is halved when the osteonal axis is perpendicular relative to its orientation parallel to the static field. These observations suggest an average alignment of the collagen fibers with the principal loading axis as observed in histologic studies of collagen fiber orientation in bone (50). We note that the quadrupolar

splittings reported here are several times larger than those reported for tendon and cartilage (36,45), which is consistent with the increased collagen fiber rigidity in bone.

Both human and lamb bone specimens exhibited a second smaller quadrupolar splitting in the ^{2}H IP-DQF spectra at τ = 400 μs, comparable to previous reports of two splittings in the calcified and radial regions of articular cartilage where it had been shown that the smaller splitting did not arise from calcium ions affecting the quadrupolar splittings (45). The origin of the second splitting requires further investigation, but may arise from collagen fibers differing in orientation, level of hydration or density.

Measurement of collagen-bound and pore BW fractions with ^{2}H IR-NMR

As quadrupolar splittings from collagen-bound BW could be plainly observed, it was clear that ^{2}H NMR was better suited than proton NMR for quantification of pore and collagen-bound BW fractions. Given the increased intra-cortical porosity occurring in osteoporotic bone loss (52) and the observation that lamb bone has different pore structure (Figure 5) (51), we decided to focus on human bone in this part of the work. It can be seen from the μCT images (Figure 4) that human bone showed the expected increase in porosity with age. Both the calculated NMR and μCT porosities were in good agreement with reported microradiographic measurements (52-53).

The present ^{2}H IR-NMR method is able to unambiguously identify and quantify collagen-bound and pore BW. The results indicate 60-80% of bulk BW to be bound to collagen, contrary to previous notions (3,22). Pore BW fractions showed significant positive correlation with porosity whereas the association of collagen-bound BW with porosity was negative. The latter relationship follows from the fact that collagen-bound BW parallels the matrix fraction, which decreases with increasing porosity. Collagen-bound BW content is expected to be inversely proportional to mineralization density. It has previously been shown that bulk BW is negatively correlated with mineralization density (3,11,54) supporting the idea that mineral displaces BW during mineralization. As we have shown that the majority of bulk BW is collagen-bound, it is reasonable to infer that collagen-bound BW is inversely proportional to mineralization. However, further investigation is warranted to distinguish the effects of pore BW, which should also be inversely proportional to mineralization.

These results highlight the opposing contributions of collagen-bound and pore BW to the bulk BWC. However, despite this complication, our bulk BWC measurements, which were in good agreement with those measured *in vivo* (22,55), showed significant positive correlation with porosity. Literature reports correlating bulk BWC with porosity are scarce, but seem to support our observation of a positive correlation. In a small pilot study Techawiboonwong et al. in patients differing in menopausal status and those with renal disease found large augmentation in bulk BW in postmenopausal subjects and those with renal osteodystrophy, both known to have increased cortical porosity (22). Very recently, Bae et al., using human bone specimens, showed that there was a weak but significant positive correlation (R^2 = 0.23) between bulk BWC and porosity measured with μCT at 3T (33).

The above observations are not in conflict with our results that indicate collagen-bound and pore BW to have opposite associations with porosity. Formation of a pore through osteoclastic action results in a gain in pore BW content that more than offsets the loss from collagen-bound BW since the actual concentration of water within a newly formed pore is greater than the collagen-bound water lost from an equal volume of osteoid. Therefore, bulk BWC would be expected to increase with porosity.

Perhaps the most important result is the strong positive correlation between NMR porosity, calculated from pore BW fraction, and μCT derived porosity. As mentioned above, both the NMR and μCT porosities fall within the reported range for a given age and sex (52-53). The slope of the line of best fit is close to unity although the y-intercept suggests that NMR porosity values tend to be ~20% larger than μCT derived porosity. A likely explanation is that at our μCT resolution of 16×16×16 μm^3, μCT derived porosity could only account for large vascular canals and did not include lacunae or canaliculi. The present NMR method does not have any spatial resolution restrictions in that it can detect pore BW in all pores. Therefore, it is to be expected that NMR-derived porosity values exceed those obtained by μCT. This high degree of agreement between NMR and μCT porosity is, to the best of our knowledge, the first experimental evidence supporting the hypothesis that pore BW is predominantly free water, whereas BW in the bone matrix is predominantly collagen-bound.

While the NMR method used here is not translatable to *in vivo* studies, it may be an important tool for the study of BW as well as for the development of new MRI methods to quantify BW. As it does not rely on Laplace inversion, the method can unambiguously quantify collagen-bound and pore BW. The ^2H NMR technique proved useful as a means to separate pore and collagen-bound BW.

In summary, we showed that ^1H and ^2H NMR can provide insight into bone micro-architecture and collagen fiber organization, allowing for unambiguous separation of pore and collagen-bound BW and quantification of porosity. The results also provided the first experimental evidence that pore BW is predominantly free, as opposed to matrix water, which is predominantly collagen-bound.

Acknowledgments

This work was supported by NIH R01 AR50068. We would also like to thank Dr. A. Tatiparthi and Dr. T. Sledz for their assistance in acquiring the μCT images with the SkyScan 1172 system.

Author's roles: Study design: HHO and FWW. Data collection: HHO and ACW. Data analysis: HHO and ACW. Data interpretation: HHO, ACW, and FWW. Drafting manuscript: HHO and FWW. Revising manuscript content: HHO, ACW, and FWW. Approving final version of manuscript: HHO, ACW, and FWW. HHO takes responsibility for the integrity of the data analysis.

References

1. Rho JY, Kuhn-Spearing L, Zioupos P. Mechanical properties and the hierarchical structure of bone. Med Eng Phys. 1998; 20:92–102. [PubMed: 9679227]
2. Martin RB. Porosity and specific surface of bone. Critical reviews in biomedical engineering. 1984; 10:179. [PubMed: 6368124]
3. Elliott SR, Robinson RA. The water content of bone. I. The mass of water, inorganic crystals, organic matrix, and CO2 space components in a unit volume of the dog bone. J Bone Joint Surg Am. 1957; 39-A:167–188. [PubMed: 13385272]
4. Piekarski K, Munro M. Transport mechanism operating between blood supply and osteocytes in long bones. Nature. 1977; 269:80–82. [PubMed: 895891]
5. Currey JD. The effects of drying and re-wetting on some mechanical properties of cortical bone. Journal of biomechanics. 1988; 21:439–441. [PubMed: 3417696]
6. Knothe T, Melissa L, Knothe ULF, Niederer P. Experimental elucidation of mechanical load-induced fluid flow and its potential role in bone metabolism and functional adaptation. The American journal of the medical sciences. 1998; 316:189. [PubMed: 9749561]
7. Rauber A Elasticität und Festigkeit der Knochen: anatomisch-physiologische Studie. Engelmann. 1876.
8. Hammett FS. A biochemical study of bone growth: I. changes in the ash, organic matter, and water during growth (*mus norvegicus albinus*). J Biol Chem. 1925; 64:409–428.

9. Timmins PA, Wall JC. Bone water. Calcif Tissue Res. 1977; 23:1–5. [PubMed: 890540]
10. Fernandez-Seara MA, Wehrli SL, Wehrli FW. Diffusion of exchangeable water in cortical bone studied by nuclear magnetic resonance. Biophys J. 2002; 82:522–529. [PubMed: 11751339]
11. Fernandez-Seara MA, Wehrli SL, Takahashi M, Wehrli FW. Water content measured by proton-deuteron exchange NMR predicts bone mineral density and mechanical properties. J Bone Miner Res. 2004; 19:289–296. [PubMed: 14969399]
12. Utku FS, Klein E, Saybasili H, Yucesoy CA, Weiner S. Probing the role of water in lamellar bone by dehydration in the environmental scanning electron microscope. J Struct Biol. 2008; 162:361–367. [PubMed: 18440829]
13. LeGeros RZ, Bonel G, Legros R. Types of “H2O” in human enamel and in precipitated apatites. Calcif Tissue Res. 1978; 26:111–118. [PubMed: 737557]
14. Wilson EE, Awonusi A, Morris MD, Kohn DH, Tecklenburg MM, Beck LW. Three structural roles for water in bone observed by solid-state NMR. Biophys J. 2006; 90:3722–3731. [PubMed: 16500963]
15. Neuman, WF.; Neuman, MW. The chemical dynamics of bone mineral. Univ. of Chicago Press; Chicago: 1958. p. xip. 209
16. Nomura S, Hiltner A, Lando JB, Baer E. Interaction of water with native collagen. Biopolymers. 1977; 16:231–246. [PubMed: 831859]
17. Pineri MH, Escoubes M, Roche G. Water--collagen interactions: calorimetric and mechanical experiments. Biopolymers. 1978; 17:2799–2815. [PubMed: 728548]
18. Bella J, Brodsky B, Berman HM. Hydration structure of a collagen peptide. Structure. 1995; 3:893–906. [PubMed: 8535783]
19. Fullerton GD, Rahal A. Collagen structure: the molecular source of the tendon magic angle effect. J Magn Reson Imaging. 2007; 25:345–361. [PubMed: 17260393]
20. Seeman E, Delmas PD. Bone quality--the material and structural basis of bone strength and fragility. N Engl J Med. 2006; 354:2250–2261. [PubMed: 16723616]
21. Robson MD, Bydder GM. Clinical ultrashort echo time imaging of bone and other connective tissues. NMR Biomed. 2006; 19:765–780. [PubMed: 17075960]
22. Techawiboonwong A, Song HK, Leonard MB, Wehrli FW. Cortical bone water: in vivo quantification with ultrashort echo-time MR imaging. Radiology. 2008; 248:824–833. [PubMed: 18632530]
23. Wu Y, Hrovat MI, Ackerman JL, Reese TG, Cao H, Ecklund K, Glimcher MJ. Bone matrix imaged in vivo by water and fat suppressed proton projection MRI (WASPI) of animal and human subjects. Journal of Magnetic Resonance Imaging. 2010; 31:954–963. [PubMed: 20373441]
24. Du J, Hamilton G, Takahashi A, Bydder M, Chung CB. Ultrashort echo time spectroscopic imaging (UTESI) of cortical bone. Magnetic Resonance in Medicine. 2007; 58:1001–1009. [PubMed: 17969110]
25. Robson MD, Gatehouse PD, Bydder M, Bydder GM. Magnetic resonance: an introduction to ultrashort TE (UTE) imaging. J Comput Assist Tomogr. 2003; 27:825–846. [PubMed: 14600447]
26. Wu Y, Ackerman JL, Chesler DA, Graham L, Wang Y, Glimcher MJ. Density of organic matrix of native mineralized bone measured by water- and fat-suppressed proton projection MRI. Magn Reson Med. 2003; 50:59–68. [PubMed: 12815679]
27. Hafner S. Fast imaging in liquids and solids with the Back-projection Low Angle ShoT (BLAST) technique. Magn Reson Imaging. 1994; 12:1047–1051. [PubMed: 7997092]
28. Idiyatullin D, Corum C, Park JY, Garwood M. Fast and quiet MRI using a swept radiofrequency. Journal of Magnetic Resonance. 2006; 181:342–349. [PubMed: 16782371]
29. Horch RA, Nyman JS, Gochberg DF, Dortch RD, Does MD. Characterization of 1H NMR signal in human cortical bone for magnetic resonance imaging. Magnetic Resonance in Medicine. 2010; 64:680–687. [PubMed: 20806375]
30. Horch RA, Gochberg DF, Nyman JS, Does MD. Non-invasive Predictors of Human Cortical Bone Mechanical Properties: T2-Discriminated 1H NMR Compared with High Resolution X-ray. PloS one. 2011; 6:e16359. [PubMed: 21283693]

31. Diaz E, Chung CB, Bae WC, Statum S, Znamirowski R, Bydder GM, Du J. Ultrashort echo time spectroscopic imaging (UTESI): an efficient method for quantifying bound and free water. NMR Biomed. 2011
32. Horch RA, Gochberg DF, Nyman JS, Does MD. Clinically compatible MRI strategies for discriminating bound and pore water in cortical bone. Magn Reson Med. 2012 In Press.
33. Bae WC, Chen PC, Chung CB, Masuda K, D'Lima D, Du J. Quantitative ultrashort echo time (UTE) MRI of human cortical bone: correlation with porosity and biomechanical properties. J Bone Miner Res. 2012 In Press.
34. Eliav U, Navon G. A study of dipolar interactions and dynamic processes of water molecules in tendon by 1H and 2H homonuclear and heteronuclear multiple-quantum-filtered NMR spectroscopy. J Magn Reson. 1999; 137:295–310. [PubMed: 10089163]
35. Edzes HT, Samulski ET. Cross relaxation and spin diffusion in the proton NMR of hydrated collagen. Nature. 1977; 265:521–523. [PubMed: 834303]
36. Navon G, Eliav U, Demco DE, Blümich B. Study of order and dynamic processes in tendon by NMR and MRI. Journal of Magnetic Resonance Imaging. 2007; 25:362–380. [PubMed: 17260401]
37. Cooper RR, Milgram JW, Robinson RA. Morphology of the osteon. An electron microscopic study. J Bone Joint Surg Am. 1966; 48:1239–1271. [PubMed: 5921783]
38. Meiboom S, Gill D. Modified spin echo method for measuring nuclear relaxation times. Review of Scientific Instruments. 1958; 29:688–691.
39. Ni Q, Nyman JS, Wang X, De Los Santos A, Nicolella DP. Assessment of water distribution changes in human cortical bone by nuclear magnetic resonance. Measurement Science and Technology. 2007; 18:715.
40. Nyman JS, Ni Q, Nicolella DP, Wang X. Measurements of mobile and bound water by nuclear magnetic resonance correlate with mechanical properties of bone. Bone. 2008; 42:193–199. [PubMed: 17964874]
41. Fantazzini P, Viola R, Alnaimi SM, Strange JH. Combined MR-relaxation and MR-cryoporometry in the study of bone microstructure. Magnetic resonance imaging. 2001; 19:481–484. [PubMed: 11445335]
42. Wang X, Ni Q. Determination of cortical bone porosity and pore size distribution using a low field pulsed NMR approach. J Orthop Res. 2003; 21:312–319. [PubMed: 12568964]
43. Epstein CL, Schotland J. The Bad Truth about Laplace's Transform. SIAM Review. 2008; 50:504–520.
44. Prange M, Song YQ. Quantifying uncertainty in NMR T2 spectra using Monte Carlo inversion. Journal of Magnetic Resonance. 2009; 196:54–60. [PubMed: 18952474]
45. Shinar H, Navon G. Multinuclear NMR and microscopic MRI studies of the articular cartilage nanostructure. NMR in Biomedicine. 2006; 19:877–893. [PubMed: 17075957]
46. Eliav U, Navon G. Multiple quantum filtered NMR studies of the interaction between collagen and water in the tendon. Journal of the American Chemical Society. 2002; 124:3125–3132. [PubMed: 11902901]
47. Cane V, Marotti G, Volpi G, Zaffe D, Palazzini S, Remaggi F, Muglia MA. Size and density of osteocyte lacunae in different regions of long bones. Calcif Tissue Int. 1982; 34:558–563. [PubMed: 6819077]
48. Wennerstroem H. Proton Nuclear Magnetic-Resonance Lineshapes in Lamellar Liquid-Crystals. Chemical Physics Letters. 1973; 18:41–44.
49. Giraud-Guille MM. Twisted plywood architecture of collagen fibrils in human compact bone osteons. Calcif Tissue Int. 1988; 42:167–180. [PubMed: 3130165]
50. Weiner S, Traub W, Wagner HD. Lamellar bone: structure-function relations. J Struct Biol. 1999; 126:241–255. [PubMed: 10475685]
51. Pearce AI, Richards RG, Milz S, Schneider E, Pearce SG. Animal models for implant biomaterial research in bone: a review. Eur Cell Mater. 2007; 13:1–10. [PubMed: 17334975]
52. Bousson V, Bergot C, Meunier A, Barbot F, Parlier-Cuau C, Laval-Jeantet AM, Laredo JD. CT of the middiaphyseal femur: cortical bone mineral density and relation to porosity. Radiology. 2000; 217:179–187. [PubMed: 11012442]

53. Laval-Jeantet AM, Bergot C, Carroll R, Garcia-Schaefer F. Cortical bone senescence and mineral bone density of the humerus. Calcif Tissue Int. 1983; 35:268–272. [PubMed: 6871757]
54. Anumula S, Wehrli SL, Magland J, Wright AC, Wehrli FW. Ultra-short echo-time MRI detects changes in bone mineralization and water content in OVX rat bone in response to alendronate treatment. Bone. 2010; 46:1391–1399. [PubMed: 20096815]
55. Techawiboonwong A, Song HK, Wehrli FW. In vivo MRI of submillisecond T(2) species with two-dimensional and three-dimensional radial sequences and applications to the measurement of cortical bone water. NMR Biomed. 2008; 21:59–70. [PubMed: 17506113]

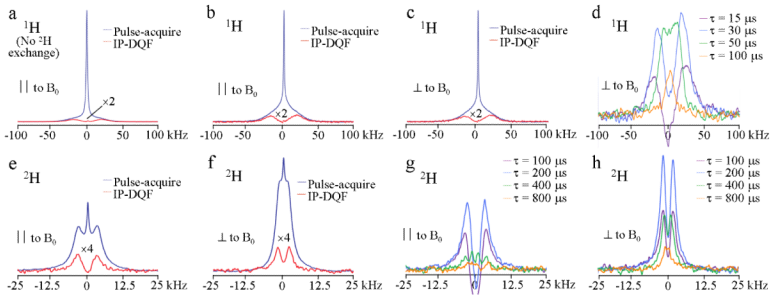

Figure 1.

Sample NMR spectra from a lamb tibia cortical bone specimen recorded at 20°C. All spectra show similar behavior over a range of temperatures (5-50°C). a): ^{1}H pulse-acquire and IP-DQF (at creation time, τ = 25 μs) spectra before ^2H_2O immersion; b, c): ^{1}H pulse-acquire and IP-DQF spectra after ^2H_2O immersion with bone parallel (∥) and perpendicular (⊥) to the applied field, B_0. Note increased vertical scale relative to panel a to highlight the dipolar splitting. d): ^{1}H IP-DQF spectra at various values of τ. e, f): ^{2}H pulse-acquire and IP-DQF (τ = 200μs) spectra after ^2H_2O immersion with bone ∥ and ⊥ to B_0. g, h): ^{2}H IP-DQF spectra at various τ for ∥ and ⊥ orientations.

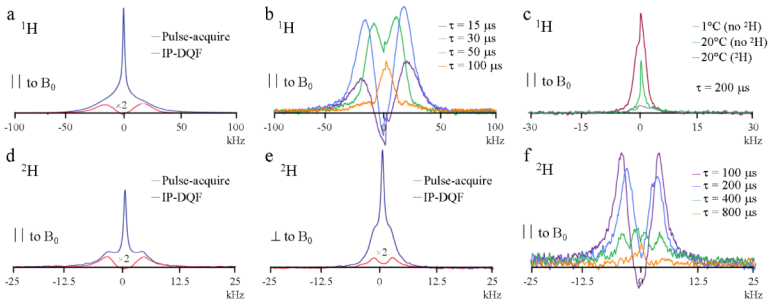

Figure 2.

NMR spectra of an anterior sample of a cortical bone specimen of the mid-shaft tibia from a 37-year old male donor after equilibration in ^2H_2O recorded at 20°C. All spectra showed similar behavior over a range of temperatures (5-50°C). a) ^{1}H pulse-acquire and IP-DQF (at creation time, τ = 25μs) spectra with the bone's longitudinal axis aligned parallel (∥) to the magnetic field, B_0. b): ^{1}H IP-DQF spectra at various τ. c): ^{1}H IP-DQF spectra (τ = 200μs) collected under various conditions. 'No ^{2}H' and '^{2}H' refer to with and without ^2H_2O immersion. d) and e): ^{2}H pulse-acquire and IP-DQF (τ = 200 μs) spectra with the bone's longitudinal axis aligned ∥ and perpendicular (⊥) to B_0. f): ^{2}H IP-DQF spectra at various τ.

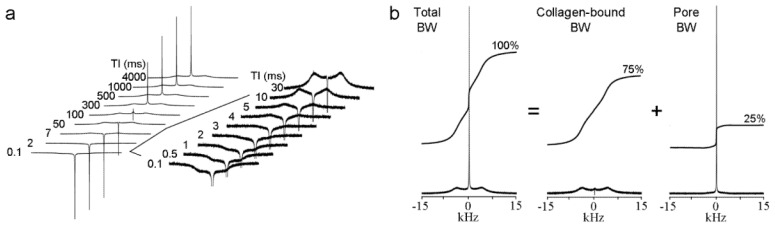

Figure 3.

Sample ^{2}H NMR spectra from the specimen the data in Fig. 2 were taken: a) IR spectra as a function of TI with the region from TI = 0.1 - 30 ms expanded. b) Spectra taken at TI=4000 ms for total, collagen-bound, and pore BW with relative integral traces.

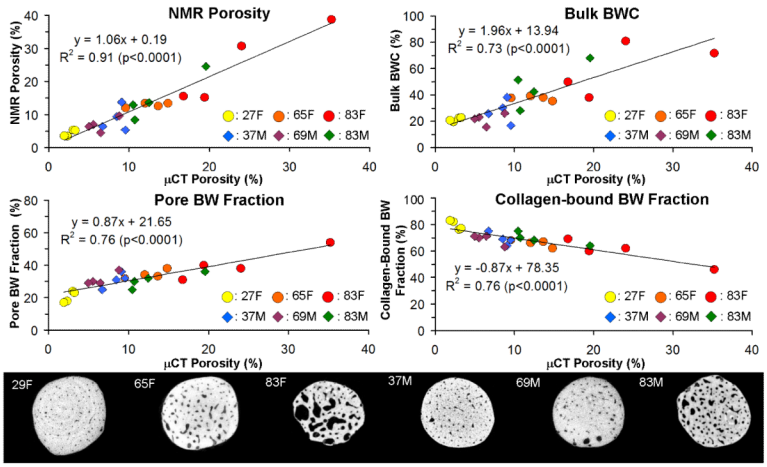

Figure 4.

Top: correlations of NMR porosity, bulk BWC, mobile BW fraction, versus μCT porosity. Circles and diamonds represent female and male donor specimens, respectively. Bottom: sample axial slices from 3D μCT images (16 μm^3 voxel size) of male (37y, 69y, 83y) and female (27y, 65y, 83y) anterior bone specimens.

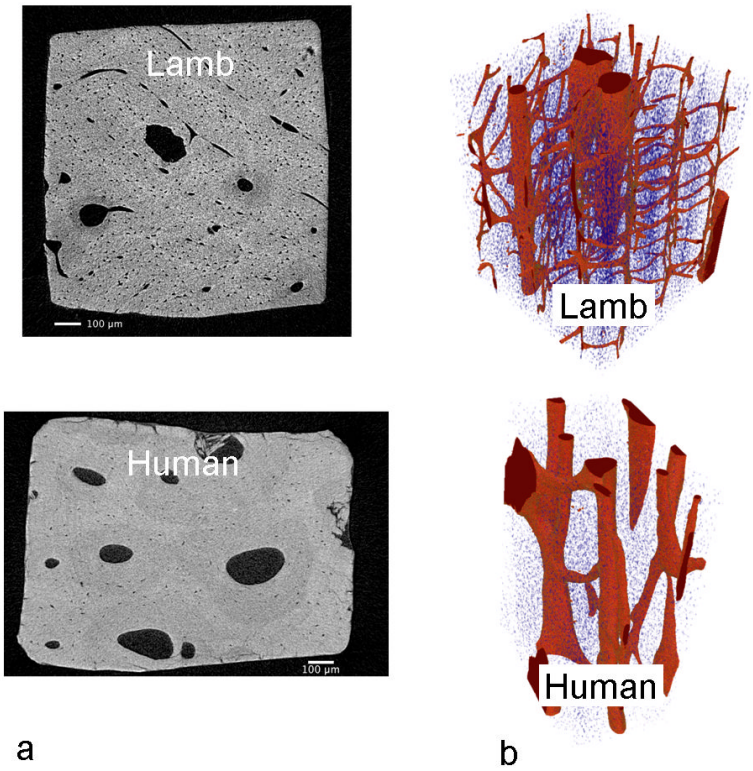

Figure 5.
a) High-resolution μCT from isotropic 3D volume data sets (1 μm^3 voxel size) from lamb and human specimens (65 y.o. female), reconstructed in the transverse plane perpendicular to osteonal axis; b) Volume rendering showing Haversian and Volkman's canals (red) and of osteocyte lacunae (blue).